Article

NMR-Detected Brownian Dynamics of αB-Crystallin over a Wide Range of Concentrations

Matthias Roos,[1] Susanne Link,[1] Jochen Balbach,[1] Alexey Krushelnitsky,[1,*] and Kay Saalwächter[1,*]
[1]Institut für Physik, Martin-Luther-Universität Halle-Wittenberg, Halle (Saale), Germany

ABSTRACT Knowledge about the global translational and rotational motion of proteins under crowded conditions is highly relevant for understanding the function of proteins in vivo. This holds in particular for human αB-crystallin, which is strongly crowded in vivo and inter alia responsible for preventing cataracts. Quantitative information on translational and rotational diffusion is not readily available, and we here demonstrate an approach that combines pulsed-field-gradient NMR for translational diffusion and proton $T_{1\rho}/T_2$ relaxation-time measurements for rotational diffusion, thus overcoming obstacles encountered in previous studies. The relaxation times measured at variable temperature provide a quantitative measure of the correlation function of protein tumbling, which cannot be approximated by a single exponential, because two components are needed for a minimal and adequate description of the data. We find that at high protein concentrations, rotational diffusion is decoupled from translational diffusion, the latter following the macroscopic viscosity change almost quantitatively, resembling the behavior of spherical colloids. Analysis of data reported in the literature shows that well-packed globular proteins follow a scaling relation between the hydrodynamic radius and the molar mass, $R_h \sim M^{1/d}$, with a fractal dimension of $d \sim 2.5$ rather than 3. Despite its oligomeric nature, R_h of αB-crystallin as derived from both NMR methods is found to be fully consistent with this relation.

INTRODUCTION

In a living cell, proteins exist and function in a rather concentrated solution of a wide range of different solutes. In comparison with dilute conditions, such crowding can significantly alter the protein behavior (1,2). The most important parameters in describing protein overall Brownian motion are the translational and rotational diffusion coefficients. Obviously, crowding increases the viscosity of the solution and slows down protein diffusion. However, this differs from a simple increase of the solution viscosity by adding, for instance, glycerol (3). Intermolecular protein interactions and their influence on Brownian diffusion are rather complicated in nature, which cannot be effectively described by increased viscosity alone. The complex changes of the protein dynamics at high protein concentrations, and the key factors determining these changes, are largely unclear at present. Experimental data on this topic are still rather sparse. Some results even contradict each other; for example, fluorescence data demonstrate that upon increasing protein concentration, translational diffusion is slowed down to a larger extent than rotational diffusion (4), whereas NMR experiments yield the opposite conclusion (3).

The interior of the vertebrate eye lens is a typical example of a crowded protein solution. Here, a highly concentrated mixture of short-range ordered (5) α-, β-, and γ-crystallins provides a high refractive index and lens transparency without protein metabolism (6,7). The main constituent of this protein mixture is α-crystallin, which comprises ~35% (w/w) of the lens crystallins (8). α-crystallin consists of two homologous proteins, αA- and αB-crystallin, which have a monomer molecular mass of ~20 kDa each. They form oligomeric associations with a molecular mass distribution from 500 to >1000 kDa and an average mass of ~800 kDa (9). Besides maintaining the high refractive index, α-crystallin acts as a molecular chaperone, preventing protein aggregation that causes cataracts to form (10,11).

Although αB-crystallin has been studied quite intensively over the last decades (for reviews, see Narberhaus (12), Horwitz (13), Augusteyn (14), and Andley (15)), its dynamics, especially at high concentrations, has not been investigated in much detail. Delaye et al. concluded that α-crystallin acts as a good model system for colloids with an effective hard-sphere radius that is not dependent on concentration (16,17), with translational self-diffusion coefficients (SDCs) that closely follow the macroscopic viscosity (18). Conversely, another report indicated that α-crystallin does not form a compact sphere at all (17) but has a dynamic quaternary structure (19).

Here, we present a detailed comparative study of the rotational and translational diffusion of αB-crystallin as a function of concentration. The translational and rotational dynamics of αB-crystallin were studied by pulsed-field-gradient (PFG) NMR and proton NMR relaxation-time measurements, respectively. PFG NMR provides an objective and robust measure of the SDC, even at high concentrations

Submitted May 15, 2014, and accepted for publication November 11, 2014.
*Correspondence: krushelnitsky@physik.uni-halle.de or kay.saalwaechter@physik.uni-halle.de
Editor: Patrick Loria.

0006-3495/15/01/0098/9 $2.00
http://dx.doi.org/10.1016/j.bpj.2014.11.1858

where dynamic light-scattering (DLS) experiments are challenged by the appearance of a slow mode and the necessary conversion of a cooperative diffusion coefficient into an SDC (20). Due to its large aggregate size, the resonances of the rigid core of αB-crystallin are broadened beyond detection (9) and thus cannot be studied by conventional high-resolution NMR techniques. We rely instead on low-resolution ^{1}H NMR relaxation-time measurements at various concentrations and temperatures, which in fact allows us to address potential ambiguities related to the common use of the NMR T_1/T_2 relaxation-time ratio as a measure of rotational diffusion. For the relaxation measurements, we rely on an integration of the whole proton spectrum, thus analyzing the integral signal from all protein protons. We present a consistent and quantitative treatment of relaxation data in terms of a bicomponent rotational autocorrelation function. Our analysis reveals a progressive decoupling of translational and rotational motion upon an increase in concentration.

MATERIALS AND METHODS

Sample preparation

Protein expression and purification of human αB-crystallin

The human αB cDNA (construct kindly provided by Prof. Wilbert Boelens, Nijmegen Centre for Molecular Life Sciences, Gelderland, The Netherlands) was cloned into a modified, His-tag-free pET16b vector and expressed in *Escherichia coli* BL21(DE3). Protein expression and purification were performed as described in Mainz et al. (21), with minor modifications including autoinduction media (ZYM 5052) instead of minimal media (M9), microfluidizer instead of French press, an additional DNA digestion step after cell lysis, and different column materials: in place of Q-Sepharose and Superose 6, TMAE and Superdex 200, respectively, were used. The lyophilized sample was dissolved in 50 mM Na-phosphate buffer, 50 mM NaCl, and 0.002% NaN_3 D_2O buffer, pD 7.6, with prior minimization of labile protons to lower the water signal and so as not to have an impact on the solvent viscosity via isotope effects. For more details, see the Supporting Material. Hen egg white lysozyme was delivered from Sigma-Aldrich (St. Louis, MO). Similar to αB-crystallin, lysozyme was dissolved in D_2O, lyophilized, and dissolved in D_2O again for maximal removal of residual water protons.

Viscosity

Steady-shear viscosities were measured at high shear rates (1000 s^{-1}/2000 s^{-1}) using the microfluid viscometer-rheometer on chip (m-VROC, Rheosense, San Ramon, CA), which determines the sample viscosity by analyzing the pressure gradient inside of a capillary ($d = 50$ μm). The samples for the viscosity measurements were also prepared using D_2O buffer instead of H_2O.

NMR experiments

Translational diffusion and $T_{1\rho}$ measurements were conducted on a Bruker Avance II spectrometer (Billerica, MA) with a ^{1}H resonance frequency for protons of 400 MHz equipped with a Diff60 probehead. $T_{1\rho}$s were measured at spin-lock frequencies of 20, 40, and 60 kHz; the latter was measured using a resonance offset of the spin-lock field with angle θ between the B_0 and B_{1e} fields fixed to 42°. T_2 measurements were performed on a Bruker Minispec mq20 at 20 MHz ^{1}H resonance frequency. The low-resonance frequency for T_2 experiments was chosen to avoid T_2 shortening due to the chemical exchange of protein protons, which may significantly affect T_2 values at high resonance frequencies (22). For the relaxation measurements, in all cases, we employ single short-pulse excitation and a sufficiently large spectral width of 50 kHz, thus assuring that all types of protons (rigid and mobile) in the protein contribute equally to the integral signal. In all cases, the accuracy of the temperature calibration and stabilization was ±1°C. For more details, see the Supporting Material.

Translational SDCs were obtained from the PFG NMR diffusion decays using the well-known formula (23)

$$A(g) = A(0) \times \exp\left(-\gamma^2 g^2 D \delta^2 (\Delta - \delta/3)\right), \quad (1)$$

where $A(g)$ is the signal intensity, g is the field gradient strength, γ is the proton gyromagnetic ratio, Δ is the diffusion time, δ is the duration of the field gradient pulse, and D is the SDC.

Rotational correlation times were obtained by analyzing NMR relaxation times. These are determined by the spectral density function, which is the Fourier transformation of the rotational autocorrelation function (RACF). The RACF of protein motion in solution is complicated in nature. For its unambiguous determination from experimental data, multiple measurements of relaxation times at different resonance frequencies are required, since each relaxation time reflects molecular dynamics only within the frequency domain around the circular (i.e., multiplied by 2π) resonance frequency. Because of the high molecular mass of the αB-crystallin oligomer, its Brownian tumbling is very slow, and thus, the often employed T_1 relaxation times are not useful for studying such a slow motion since they provide information on (sub)nanosecond-timescale motions, which is much faster than the αB-crystallin tumbling. For this reason, we used $T_{1\rho}$ proton relaxation times, which enable one to shift the sampling frequency of motions down to the 10–100 kHz range. Specifically, we measured the temperature dependences of $T_{1\rho}$ values at spin-lock frequencies (the analog of the resonance frequency for T_1) of 20, 40, and 60 kHz, the latter values being measured using the resonance offset of spin-lock irradiation (see the Supporting Material). We stress that measuring relaxation times at different temperatures is important for a reliable data analysis, since the slope of the temperature dependence is more informative than the absolute value of the relaxation time measured at one temperature in correctly determining the rotational correlation time. In addition to $T_{1\rho}$ values, we also measured the proton T_2, which provides the low-frequency limit of the spectral density function. The relaxation is governed by the homonuclear (^{1}H-^{1}H) dipole-dipole mechanism; all other mechanisms are negligible in this case. The equations for the homonuclear dipolar T_1, T_2, and $T_{1\rho}$ relaxation times are well known (24). However, since we measured off-resonance $T_{1\rho}$, for the data analysis, we should use a general expression defining relaxation times T_1 and $T_{1\rho}$ at arbitrary off-resonance angle. Such an expression was derived a long time ago by Jones (25). In a more compact form, applying the approximation $\omega_0 >> \omega_{1e}$, this expression reads (26)

$$\frac{1}{T_{1\rho}} = \frac{1}{T_1} + \sin^2\theta \left[\frac{1}{T_{1\rho}^{\Delta}} - \frac{3}{4T_1}\right], \quad (2)$$

where

$$\frac{1}{T_1} = \frac{2}{3} K_{HH}\left(J(\omega_0) + 4J(2\omega_0)\right), \quad (3)$$

$$\frac{1}{T_{1\rho}^{\Delta}} = K_{HH}\left(\cos^2\theta \times J(\omega_{1e}) + \sin^2\theta \times J(2\omega_{1e}) + \frac{3}{2}J(\omega_0)\right). \quad (4)$$

Here, θ is the off-resonance angle (the angle between the static field B_0 and effective spin-lock field B_{1e}), $J(\omega)$ is the spectral density function, K_{HH} is the squared effective proton-proton dipolar coupling (second moment), and $\omega_0/2\pi$ and $\omega_{1e}/2\pi$ are the resonance and spin-lock frequencies, respectively. At $\theta = 0^\circ$ and 90°, Eq. 2 converts to the standard expressions for T_1 and $T_{1\rho}$, respectively. Relaxation time T_2 corresponds to the case $\theta = 90^\circ$ and $\omega_{1e} = 0$. Note that these equations are valid not only in the fast-motion limit, but for slow motions as well (27). For the case of the relaxation of protein protons, the effective K_{HH} can be expressed as

$$K_{HH} = \frac{9}{20} \times \frac{1}{N} \times \hbar^2\gamma^4 \sum_{i \neq j} r_{ij}^{-6}, \quad (5)$$

where N is the number of protons in a protein, $\hbar$ is the Planck constant, γ is the proton gyromagnetic ratio, and r_{ij} is the distance between the ith and jth protons in the protein. Although summation in Eq. 5 formally extends over all protons in the protein, because of the r^{-6} dependence, the dominant contribution to the coupling for each proton is attributable to the two to three nearest neighbors, and proton-proton interactions with more distant neighbors are practically negligible.

Since an integral proton signal was detected in the relaxation experiments, the spectral density function $J(\omega)$ in Eqs. 2–4 is the average spectral density of all protons in the protein:

$$J(\omega) = \frac{1}{N}\sum J_i(\omega). \quad (6)$$

The same is true for the RACF:

$$C(t) = \frac{1}{N}\sum C_i(t). \quad (7)$$

Each individual RACF can be written as a product of the correlation functions of the overall Brownian tumbling and internal local motion (28),

$$\begin{aligned} C_i(t) &= C_t(t) \times C_{li}(t) \\ &= C_t(t) \times \left[S_{li}^2 + \left(1 - S_{li}^2\right)\exp\left(-\frac{t}{\tau_{li}}\right)\right], \end{aligned} \quad (8)$$

where $C_t(t)$ is the overall tumbling RACF and S_{li}^2 and τ_{li} are the order parameter and correlation time of the internal motion for the ith proton. Since $C_t(t)$ is the same for all protons, Eq. 7 can be rewritten as

$$C(t) = C_t(t) \times \left[S_l^2 + \frac{1}{N}\sum\left(1 - S_{li}^2\right)\exp\left(-\frac{t}{\tau_{li}}\right)\right], \quad (9)$$

where $S_l^2 = 1/N\sum S_{li}^2$. Then, the spectral density function is

$$J(\omega) = S_l^2 J_t(\omega) + \frac{1}{N}\sum \frac{\left(1 - S_{li}^2\right)\tau_{li}}{1 + (\omega\tau_{li})^2}, \quad (10)$$

where $J_t(\omega)$ is the Fourier transform of $C_t(t)$. In our analysis, we assume that all values of τ_{li} are much smaller than the correlation time of the overall protein tumbling. Then, the second term in Eq. 10 can be neglected. This formalism is very similar to that applied in the analysis of field-cycling T_1 relaxation data of protein protons in D_2O solutions (29).

The key point of our analysis is an assumption of a biexponential overall tumbling RACF $C_t(t)$. Even in relatively dilute protein solutions, long-range electrostatic intermolecular protein interactions give rise to a local anisotropy that renders the so-called normal Brownian tumbling somewhat anisotropic (30,31). Thus, the RACF decays not to zero, but to a certain value that we denote as the rotational order parameter, S_{rot}^2. Its physical meaning is similar to that of the order parameter of the internal motions (28): both are measures of the anisotropy of rotational motion of the overall tumbling and internal mobility, respectively. In infinitely dilute solutions, $S_{rot}^2 = 0$, and it increases with increasing concentration, as interprotein interactions become stronger and Brownian tumbling thus becomes more anisotropic. Since proteins diffuse relative to each other, the local anisotropy has a finite lifetime; hence, $C_t(t)$ finally decays to zero, but on a longer timescale than for normal Brownian tumbling. Therefore, $C_t(t)$ can be presented as a sum of two components,

$$C_t(t) = \left(1 - S_{rot}^2\right)\exp(-t/\tau_{rot}) + S_{rot}^2\exp(-t/\tau_S), \quad (11)$$

where τ_{rot} is the correlation time of Brownian rotation and τ_S is the correlation time of the slow component of $C_t(t)$, i.e., the lifetime of local anisotropy. The apparent slow contribution to protein Brownian tumbling has been observed experimentally and computationally in a number of independent works (for a review, see Krushelnitsky (31)).

The corresponding spectral density function reads

$$J_t(\omega) = \frac{\left(1 - S_{rot}^2\right)\tau_{rot}}{1 + (\omega\tau_{rot})^2} + \frac{S_{rot}^2\tau_S}{1 + (\omega\tau_S)^2}. \quad (12)$$

For typical protein concentrations of high-resolution NMR samples (a few mM), S_{rot}^2 is very low, less than a few percent (31). Hence, T_1 relaxation times are not sensitive to the slow component. However, T_2s are quite sensitive to it because of the spectral density function at zero frequency:

$$J_t(0) = \left(1 - S_{rot}^2\right)\tau_{rot} + S_{rot}^2\tau_S. \quad (13)$$

Despite the fact that $S_{rot}^2 << 1$, the two terms in Eq. 13 are comparable, since $\tau_S >> \tau_{rot}$. For this reason, using the T_1/T_2 ratio for determination of the tumbling correlation time, τ_{rot}, can provide imprecise results. The higher the concentration, the less correct is the value of τ_{rot} obtained from the T_1/T_2 ratio. Thus, the assumption of a biexponential form of $C_t(t)$ is a prerequisite for the correct analysis of the relaxation data at different concentrations.

In fitting the temperature dependences of the relaxation times, we assume an Arrhenius dependence of the correlation times,

$$\tau_{S,rot} = \tau_{S,rot}(293K)\exp\left[\frac{E_{S,rot}}{R}\left(\frac{1}{T} - \frac{1}{293K}\right)\right], \quad (14)$$

where $E_{S,rot}$ is the activation energy of the τ_S/τ_{rot} correlation times and R is the universal gas constant. Thus, the fitting parameters in the analysis were two correlation times, two activation energies, the order parameter S_{rot}^2 (separate sets for each concentration), and the product of the rigid-lattice second moment, K_{HH} (which for rigid globular proteins has an approximate value of ~1.3×10^{10} s^{-2} (32)), and the order parameter S_l^2:

$$K_{HH}^{av} = S_l^2 K_{HH}, \quad (15)$$

where K_{HH}^{av} is the motionally averaged second moment of the protein protons; we assume it to be the same for all concentrations. The overall number of the fitting parameters for all four concentrations was 21: five parameters for each concentration (see above) and one parameter (K_{HH}^{av}) shared between all concentrations. For the fitting, we used Eqs. 2–4, replacing $J(\omega)$ and K_{HH} by $J_t(\omega)$ and K_{HH}^{av}, respectively. A similar approach was taken previously by Bertini et al. (29), stressing the use of S_l^2 as a qualitative indicator of internal rigidity. For simplicity, we assume S_{rot}^2 to be temperature-independent and we neglect the distribution of sizes. Strictly speaking, this is not absolutely true, yet it has only a minor effect on the analysis, as demonstrated in Fig. S8. K_{HH}^{av} is also assumed to be temperature-independent. Within the temperature range of our experiments, the temperature dependence of K_{HH}^{av} is rather weak (32,33). Simply assuming a reasonable temperature dependence, however, has practically no influence on the results (see Table S2).

The fitting procedure was based upon a minimization of the root mean-square deviation,

$$\mathrm{RMSD} = \sqrt{\frac{1}{N}\sum_{i=1}^{N}\left(\frac{T_{\mathrm{sim}} - T_{\mathrm{exp}}}{T_{\mathrm{exp}}}\right)^2}, \qquad (16)$$

where T_{sim} and T_{exp} are the simulated (according to the current set of the fitting parameters) and experimental relaxation times ($T_{1\rho}$ or T_2), respectively, and N is the number of all relaxation times measured at all temperatures and concentrations. For the minimization procedure, we used the Metropolis algorithm.

RESULTS

Translational diffusion and viscosity

Typical examples of the PFG NMR intensity decays (signal intensity versus strength of the pulsed field gradient) are shown in Fig. 1. In the representation $\log(I)$ versus g^2, a deviation of the intensity decay from a straight line reflects an SDC dispersion, i.e., a distribution of molecular mass. Fig. 1 likewise demonstrates that this distribution is somewhat wider for a higher concentration; the normalized (relative) RMSDs of the diffusion coefficients from their average, as estimated from a bicomponent decomposition of the decays, are 0.2, 0.2, 0.25, and 0.35 for the concentrations 35, 80, 113, and 185 mg/mL, respectively, in qualitative agreement with DLS data (20). In this analysis we did not quantify the distribution, instead defining the mean SDC, which corresponds to the initial slope of the decay. Practically, we fitted the decay with a sum of two components as a minimal but sufficient model and then calculated the mean SDC as

$$\langle D \rangle = (P_1 \times D_1 + P_2 \times D_2)/(P_1 + P_2), \qquad (17)$$

where $P_{1,2}$ and $D_{1,2}$ are the intensities and SDCs, respectively, of the two components. The specific values of D_1 and D_2 depend on the weighting factor; these values taken separately have no physical meaning, yet the average diffusion coefficient is well-defined and reliable. Note that the subunit exchange between α-crystallin oligomers occurs on a timescale of minutes (34); thus, the observed SDC is not the exchange-averaged value of SDCs of oligomers and mono(di)mers. In fact, the amount of α-crystallin mono(di)meric subunits in solution is very low; otherwise, we would see a corresponding fast component in the PFG intensity decays.

Fig. 2 *a* presents the temperature dependences of mean SDCs at four different concentrations of αB-crystallin in an Arrhenius representation. It is useful to analyze these data in comparison with lysozyme (M = 14.3 kDa). At acidic pH, lysozyme forms no dimers or oligomers and retains its rigid native structure over a wide range of concentrations and temperatures (35). This comparison shows that the slope of the SDC temperature dependences (i.e., the activation energy of translational diffusion) for αB-crystallin at all concentrations is quite similar to that of lysozyme. This indicates that at all concentrations, the mean molecular mass of the αB-crystallin assemblies is independent of temperature. Fig. 2 *b* presents the macroscopic viscosity, along with data for pure D_2O. In the Arrhenius plot, given the

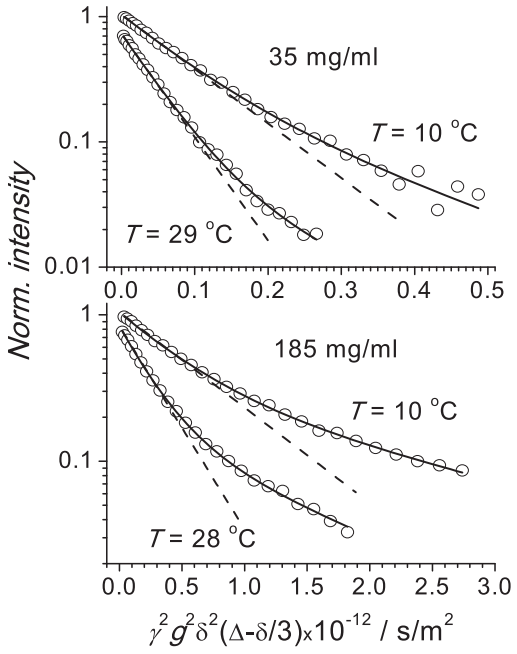

FIGURE 1 Typical examples of diffusion-dependent PFG NMR decays of αB-crystallin at two different concentrations and two different temperatures. The experimental error corresponds to the size of the symbols in the initial part of the decays. Solid red lines are bicomponent fits of the decays and dashed lines denote the initial slope of the decays corresponding to the mean SDC.

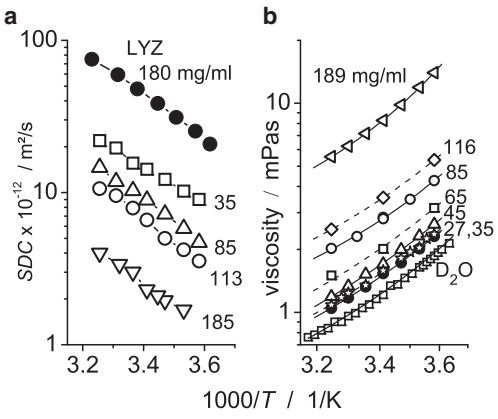

FIGURE 2 Translational self-diffusion coefficients and viscosity of αB-crystallin. In both graphs, the size of the symbols corresponds to the experimental uncertainty. (*a*) Temperature dependences of the mean SDCs at four different concentrations of αB-crystallin (*open symbols*). For comparison, SDCs of a lysozyme solution (concentration 180 mg/mL, pD 3.5) are shown (*solid symbols*). (*b*) Temperature dependence of the viscosity at seven concentrations of αB-crystallin (*symbols*), displaying a Vogel-Fulcher relationship (*solid lines*). The solid line for the D_2O viscosity represents literature data as recalculated (48) from the viscosity of water (49).

improved data quality of the viscosity measurements compared to those of translational diffusion, a slight curvature of the viscosity can be seen, indicating that the glassy dynamics related to the solvent can be described by a Vogel-Fulcher relationship (36). A slightly stronger deviation from the Arrhenius behavior is observed for the highest concentrations, pointing to the increasing relevance of studying the glassy dynamics of confined/bound water.

At the smallest concentration (35 mg/mL), the protein SDC concentration dependence is weak (37), and thus, intermolecular protein interactions have almost no influence on the SDC. This allows us to estimate the size of αB-crystallin using the Stokes-Einstein relationship and the experimental viscosity data. This gives a temperature-independent value (see Fig. S7) of $R_H = (95 \pm 3)$ Å, which exactly matches the value obtained from the DLS experiments by Licinio et al. (20). Note that those authors were studying α-crystallin from calf lenses, which are oligomers composed of a mixture of αA- and αB-crystallins.

Rotational diffusion

Fig. 3 depicts the relaxation times and fitting curves for different concentrations of αB-crystallin. Fitting a single-component correlation function for the protein Brownian rotation (i.e., assuming $S^2_{rot} = 0$) results in a pronounced mismatch, confirming the invalidity of the one-component model. The fitting results are summarized in Table 1.

The absolute value of the rotational correlation time for the lowest concentration investigated in this study, 35 mg/mL, is 0.9 μs. Applying the Stokes-Einstein-Debye law with the experimentally determined viscosity of this sample, these values correspond to an αB-crystallin radius of ~82 Å. This value is somewhat less than 95 Å, as obtained from the translational diffusion data (see above). This may indicate that the Stokes-Einstein-Debye law does not hold for the rotational diffusion, and that the macroscopic viscosity should not be used to determine rotational correlation time (see below). If, instead of the solution viscosity, the viscosity of a pure solvent (D_2O) is used in the Stokes-Einstein-Debye equation, then the calculated αB-crystallin radius reaches 89 Å. Given the overall experimental accuracy, the discrepancy between 89 Å and 95 Å can be considered as negligible. Note that the activation energy of the Brownian tumbling E_{rot} corresponds quite well to that of the viscous flow of pure water, which is ~19 kJ/mol (38). The decrease of E_{rot} to 10 kJ/mol at a concentration of 185 mg/mL is obviously an apparent effect associated with the increased distribution of molecular masses and the probably more complex form of the $C_t(t)$.

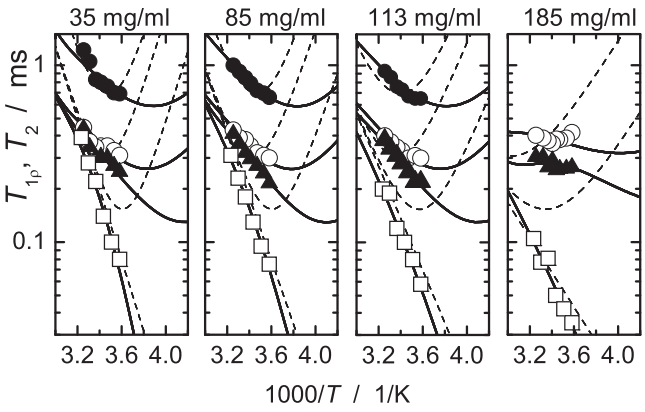

FIGURE 3 Proton $T_{1\rho}$ and T_2 for αB-crystallin solutions at different concentrations. The experimental error corresponds to the size of the symbols. Information is provided for relaxation times T_2 (*open squares*), $T_{1\rho}$ at the spin-lock frequency, 20 kHz (*solid triangles*), $T_{1\rho}$ at 40 kHz (*open circles*), and off-resonance $T_{1\rho}$ at 60 kHz (*solid circles*) (the latter parameter was not measured for 185 mg/mL). Solid lines show the best fits for double-exponential correlation functions, and dashed lines correspond to the best fit assuming $S^2_{rot} = 0$, i.e., a single-exponential correlation function.

DISCUSSION

The impact of crowding: rotational diffusion is less hindered than translational diffusion

Since the rotational diffusion is described by the two-component overall tumbling RACF $C_t(t)$, we define, as in the case of translational diffusion, a mean rotational diffusion rate $\langle R_{rot} \rangle$ equal to the initial slope of the rotational correlation function:

$$\langle R_{rot} \rangle = \frac{1 - S^2_{rot}}{\tau_{rot}} + \frac{S^2_{rot}}{\tau_S}. \quad (18)$$

Since S^2_{rot} and τ_S are poorly defined at low concentrations there is a certain ambiguity in defining the rotational diffusion rate at low concentrations. However, since the second term in Eq. 18 is much smaller than the first, this ambiguity is obviously negligible.

Fig. 4 presents the central result of this work, the comparative retardation of translational and rotational diffusion relative to macroscopic viscosity with increasing concentration. It is seen that the trend of the translational diffusion nicely corresponds to that of viscosity, which confirms previous findings by Licinio and Delaye (18). Thus, the Stokes-Einstein law appears to be valid even at high concentrations. This in turn shows that the mean size of αB-crystallin under our conditions does not depend on concentration.

On the other hand, these results clearly demonstrate a significant difference between translational and rotational diffusion of αB-crystallin at high concentrations, far beyond all the assumptions and uncertainties of the data analysis. We also stress that fitting the relaxation data with a fixed ratio of the correlation times, τ_{rot}, at different concentrations after the known increase in viscosity (and thus the slowdown of translational diffusion) results in a strong mismatch with the experimental data (see Fig. S10).

TABLE 1 Dynamic parameters obtained from the data fitting

c/mg/mL	$\tau_{rot}/\mu s$ at 20°C	S^2_{rot}	$\tau_S/\mu s$ at 20°C	$S^2_{rot}\,\tau_S/\mu s$ at 20°C	E_{rot}/kJ/mol	E_s/kJ/mol
35	0.90 ± 0.02	<0.03	>30	0.64 ± 0.02	16 ± 1	66 ± 2
85	0.96 ± 0.02	<0.03	>30	0.83 ± 0.02	18 ± 1	51 ± 2
113	1.03 ± 0.03	<0.03	>80	1.36 ± 0.03	17 ± 1	40 ± 2
185	1.04 ± 0.03	0.22 ± 0.02	17 ± 1	3.70 ± 0.06	10 ± 1	30 ± 1

K^{av}_{HH} (Eq. 15) was found to be (4.2 ± 0.2) × 10^9 s^{-2} by a shared fit of all data sets. Since S^2_{rot} is very small, the parameters S^2_{rot} and τ_S cannot be determined separately at low concentrations; only the product $S^2_{rot}\,\tau_S$ could be reliably obtained from the fitting. For details, see Krushelnitsky (31).

Interestingly, a similar conclusion regarding the limited applicability of the Stokes-Einstein-Debye law for high αB-crystallin concentrations can be deduced from recently published data on Brownian tumbling of this protein obtained by field-cycling relaxometry of the water protons (39). At a single concentration of 100 mg/mL, $T = 25°C$ in 80% H_2O and 20% glycerol solvent, the correlation time, τ_{rot}, of αB-crystallin was found to be 1.4 μs. Using our viscosity data for this protein concentration and temperature, and taking into account the correction factor for viscosity between D_2O and 80% H_2O and 20% glycerol solvents, we estimated the apparent radius of αB-crystallin to be 68 Å. This value is obviously too small, in accordance with our finding that rotational diffusion is less hindered than expected by the increase of viscosity.

Similar concentration dependences of rotational and translational protein diffusion have been reported previously (4), but this is the first time, to our knowledge, that such a large quantitative difference has been observed in a protein system. The effect of less hindered rotations compared to the translational self-diffusion goes far beyond a pure viscosity effect resulting from the difference in local microviscosity around the protein and the bulk viscosity. Increasing the bulk viscosity with ethylene glycol by a factor of 6 (corresponding to a retardation factor of 6 in Fig. 4) results in retardation of translation diffusion and rotational diffusion by factors of 5.5 and 4, respectively, for a small globular protein (40). The less hindered rotation at high protein concentrations can be easily understood in terms of the cage effect, which is well known for the case of spherical colloids (41,42). For translational diffusion, each probe molecule needs to escape a cage formed by the surrounding particles (α-relaxation) and thus has to interact with its neighboring proteins, which represent obstacles to translational motion. For rotational diffusion, proteins may rotate rather freely within a cage (β-relaxation); hence, intermolecular protein interactions can be expected to have an appreciably smaller effect on it. Note that the effect of decoupling between translational and rotational diffusion has been observed not only in experimental studies, but also in numerical simulations of protein diffusion at high concentrations (43). However, we refrain from extrapolating the findings of this work to other proteins and experimental conditions. The acquired data are obviously not sufficient to make generalizations, and more experimental work is required to further advance our knowledge in this area.

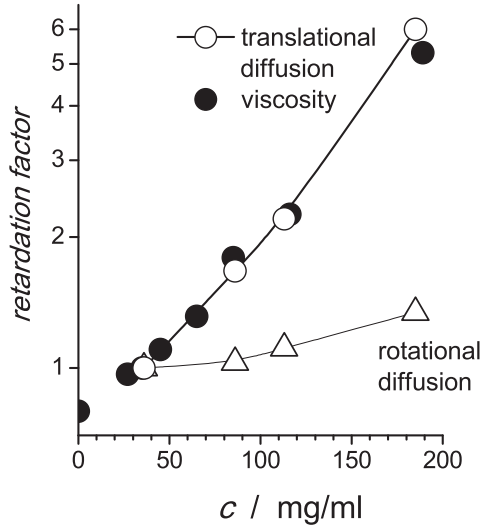

FIGURE 4 Retardation of the translational (*open circles*) and rotational diffusion (*open triangles*) as a function of αB-crystallin concentration as compared to the normalized macroscopic viscosity (*solid circles*). The retardation factor was defined as the ratio of the translational (rotational) diffusion rate to the value at 35 mg/mL, taken as a reference for the higher concentrations. The viscosity was normalized in the same way. The size of the symbols reflects the experimental error, and the solid line simply guides the eye.

Fractal structure: αB-crystallin behaves like a normal globular protein

Further information on αB-crystallin properties can be obtained by comparing the absolute values of the diffusion constants with those of other proteins. Although such data have been published, at least for translational diffusion (see, e.g., the work of Delaye and colleagues (16,18,20)), the comparison has apparently not yet been made. The SDC is inversely proportional to the linear size of the Brownian particle, whereas the rotational correlation time is proportional to its volume. To minimize the influence of intermolecular protein interactions, we compared the diffusion parameters only for the dilute αB-crystallin solution. If the average protein density is the same for proteins of different molecular mass, M, one might expect that SDC ~ $M^{-0.33}$ and τ_{rot} ~ M, but this is not the case. Computer analysis of a large number of 3D protein structures

(44,45) demonstrates that $V \sim R^d$, where V is the van der Waals (or solvent-accessible) volume of the protein directly proportional to the molecular mass, which is connected to the linear size, R (more specifically, the radius of gyration) of the protein molecule by a scaling exponent, d, of ~2.5. Such a relation between size and volume reflects a fractal nature of the protein packing, which has generated increased interest over the last few years (see the review by Banerji and Ghos (46)). The fractal dimension $d < 3$ indicates that the protein density decreases with increasing M (47). If $V \sim M$, then the SDC is $\sim M^{-1/d}$ and $\tau_{rot} \sim M^{3/d}$.

Fig. 5 *a* shows a collection of data from the literature on SDCs as a function of M for many proteins and includes the αB-crystallin results from this work. Two important points must be mentioned. First, the slope of the SDC versus M dependence matches reasonably well the value of d obtained by Liang and Dill (44). To our knowledge, this is the first experimental confirmation of this fractal dependence based on diffusion data, reporting on the hydrodynamic radius R_h. Second, the αB-crystallin SDC is located close to this line, which indicates that it has no specific features, as compared to other globular proteins, and is just as compact as might be expected based on the fractal scaling law, $R_h \sim M^{1/d}$, and its high molecular mass.

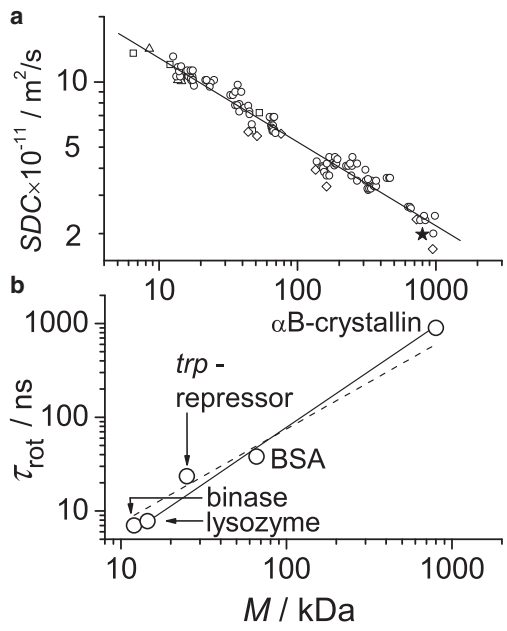

FIGURE 5 (*a*) SDCs for different proteins as a function of M at 20°C. Literature data are either taken directly from Tyn and Gusek (50) and Ilyina et al. (51) (*open circles and triangles*) or recalculated from the hydrodynamic radii reported in Wilkins et al. (52) and Armstrong et al. (53) (*open squares and diamonds*). Proteins too anisotropic in shape or that are intrinsically disordered were not taken into account. The αB-crystallin SDC as obtained in this study is indicated by the solid star. The αB-crystallin SDC was measured at a concentration of 10 mg/mL and multiplied by 1.25 to account for the viscosity difference between H_2O (literature data of H_2O solutions) and D_2O (this work). The solid line is a best fit to the data, with a slope (power-law exponent) of 0.39 ± 0.03. (*b*) Rotational correlation time τ_{rot} at 20°C for five different proteins as a function of molecular weight. The solid line presents the dependence $\tau_{rot} \sim M^{1.2}$. For comparison, the dashed line shows the dependence $\tau_{rot} \sim M$.

A similar dependence can likewise be plotted for rotational diffusion. Many studies have been published on protein dynamics in solution over the last 20 to 30 years. However, in most of these, the rotational correlation time was determined from the NMR T_1/T_2 relaxation-time ratio assuming only a single-component RACF or, at best, a more complex form of it accounting for the anisotropic shape of the protein. We again stress that this is quantitatively not correct (see above). The amplitude of the slow component of the RACF depends on many parameters (concentration, ionic strength, pH, and electrostatic properties of a protein) and hence is different for different experiments. This induces a spread of τ_{rot} values that makes it difficult to reliably define the power-law exponent of M (see Fig. S11). Therefore, for comparison, we took the data of only four proteins, binase, lysozyme, *trp*-repressor, and bovine serum albumin, as described in Krushelnitsky (31). In that study, τ_{rot} was determined according to the same protocol as in this work, so the correlation times can be compared directly.

Fig. 5 *b* presents τ_{rot} as a function of M for five proteins, including αB-crystallin. Despite the poor statistics, it can be clearly seen that rotational diffusion also confirms the findings of Liang and Dill (44). The largest deviation from the solid line in Fig. 5 *b* is observed for *trp*-repressor. This can be explained by the fact that *trp*-repressor is a symmetric dimer with two long (12 residues each) unstructured chains exposed to the solvent. Thus, the *trp*-repressor is not a completely rigid protein, and an apparently increased τ_{rot} is easily understood. Note that the rotational diffusion of αB-crystallin again reveals no evident specificity in comparison with other globular proteins.

CONCLUSIONS

In this study, we have provided an accurate determination of the translational and rotational diffusion of αB-crystallin over a wide range of concentrations. Our data allowed us to draw three important conclusions. First, our main finding was that upon increasing the protein concentration, the translational diffusion of αB-crystallin nicely followed the trend measured for the inverse solution viscosity, whereas the rotational diffusion was found to be affected by the concentration increase to a much smaller extent. This could be explained on the basis of the cage effect typical for spherical colloids. The temperature dependence of all observables was found to be largely governed by the flow activation energy of pure water, with deviations visible only at the largest concentrations. Second, despite its large size and oligomeric structure, αB-crystallin in dilute solution behaves like a normal rigid globular protein, showing no specificity in Brownian dynamics compared to other, even much smaller,

proteins. Third, both the translational and rotational diffusion data (reporting on the hydrodynamic radius, R_h) confirm the fractal scaling law, $V \sim M \sim R^d$, with $d \sim 2.5$ instead of $d \sim 3$ for a variety of protein structures of different size, R. This finding is in agreement with previous statistical analyses of protein packing density.

The methodological approach presented here, in particular addressing the autocorrelation function of the overall protein tumbling by a bimodal analysis of NMR relaxation times measured at different frequencies and temperatures, provides an efficient and reliable tool for studying the effect of crowding on Brownian dynamics. Application of this approach to the αB-crystallin study enabled a qualitative step forward in the description of protein mobility at high concentrations. We expect that the use of this approach for other proteins and protein mixtures will help in constructing a detailed and consistent general picture of protein dynamics under crowding conditions.

SUPPORTING MATERIAL

Supporting Materials and Methods, eleven figures, and three tables are available at http://www.biophysj.org/biophysj/supplemental/S0006-3495(14)03070-7.

ACKNOWLEDGMENTS

We thank Wilbert Boelens for the plasmid for αB crystallin and Qi Zhang for the expression clone.

Funding for this work was provided by the Deutsche Forschungsgemeinschaft (DFG) in the framework of the collaborative research center SFB-TRR 102 (project A08). We also acknowledge significant investments in our NMR facility by the European Regional Development Fund (ERDF) of the European Union.

REFERENCES

1. Zimmerman, S. B., and A. P. Minton. 1993. Macromolecular crowding: biochemical, biophysical, and physiological consequences. *Annu. Rev. Biophys. Biomol. Struct.* 22:27–65.
2. Ellis, R. J. 2001. Macromolecular crowding: obvious but underappreciated. *Trends Biochem. Sci.* 26:597–604.
3. Wang, Y., C. Li, and G. J. Pielak. 2010. Effects of proteins on protein diffusion. *J. Am. Chem. Soc.* 132:9392–9397.
4. Zorrilla, S., M. A. Hink, …, M. P. Lillo. 2007. Translational and rotational motions of proteins in a protein crowded environment. *Biophys. Chem.* 125:298–305.
5. Delaye, M., and A. Tardieu. 1983. Short-range order of crystallin proteins accounts for eye lens transparency. *Nature.* 302:415–417.
6. Bloemendal, H. 1977. The vertebrate eye lens. *Science.* 197:127–138.
7. Bloemendal, H., W. de Jong, …, A. Tardieu. 2004. Ageing and vision: structure, stability and function of lens crystallins. *Prog. Biophys. Mol. Biol.* 86:407–485.
8. Pierscionek, B., and R. C. Augusteyn. 1988. Protein distribution patterns in concentric layers from single bovine lenses: changes with development and ageing. *Curr. Eye Res.* 7:11–23.
9. Carver, J. A. 1999. Probing the structure and interactions of crystallin proteins by NMR spectroscopy. *Prog. Retin. Eye Res.* 18:431–462.
10. Horwitz, J. 1992. Alpha-crystallin can function as a molecular chaperone. *Proc. Natl. Acad. Sci. USA.* 89:10449–10453.
11. Derham, B. K., and J. J. Harding. 1999. α-Crystallin as a molecular chaperone. *Prog. Retin. Eye Res.* 18:463–509.
12. Narberhaus, F. 2002. α-Crystallin-type heat shock proteins: socializing minichaperones in the context of a multichaperone network. *Microbiol. Mol. Biol. Rev.* 66:64–93.
13. Horwitz, J. 2003. α-Crystallin. *Exp. Eye Res.* 76:145–153.
14. Augusteyn, R. C. 2004. α-Crystallin: a review of its structure and function. *Clin. Exp. Optom.* 87:356–366.
15. Andley, U. P. 2007. Crystallins in the eye: function and pathology. *Prog. Retin. Eye Res.* 26:78–98.
16. Delaye, M., and A. Gromiec. 1983. Mutual diffusion of crystallin proteins at finite concentrations: a light-scattering study. *Biopolymers.* 22:1203–1221.
17. Tardieu, A., D. Laporte, and M. Delaye. 1987. Colloidal dispersions of α-crystallin proteins. 1. Small-angle x-ray analysis of the dispersion structure. *J. Phys.* (*Paris*). 48:1207–1215.
18. Licinio, P., and M. Delaye. 1988. Mutual and self-diffusion in concentrated α-crystallin protein dispersion. A dynamic light-scattering study. *J. Phys. (Paris).* 49:975–981.
19. Haley, D. A., J. Horwitz, and P. L. Stewart. 1998. The small heat-shock protein, αB-crystallin, has a variable quaternary structure. *J. Mol. Biol.* 277:27–35.
20. Licinio, P., M. Delaye, …, L. Leger. 1987. Colloidal dispersions of α-crystallin proteins. 2. Dynamics: a maximum-entropy analysis of photon-correlation spectroscopy data. *J. Phys.* (*Paris*). 48:1217–1223.
21. Mainz, A., S. Jehle, …, B. Reif. 2009. Large protein complexes with extreme rotational correlation times investigated in solution by magic-angle-spinning NMR spectroscopy. *J. Am. Chem. Soc.* 131:15968–15969.
22. Luz, Z., and S. Meiboom. 1963. Nuclear magnetic resonance study of protolysis of trimethylammonium ion in aqueous solution: order of reaction with respect to solvent. *J. Chem. Phys.* 39:366–370.
23. Stejskal, E. O., and J. E. Tanner. 1965. Spin diffusion measurements: spin echoes in the presence of a time-dependent field gradient. *J. Chem. Phys.* 42:288–292.
24. Kimmich, R., and E. Anoardo. 2004. Field-cycling NMR relaxometry. *Prog. NMR Spectrosc.* 44:257–320.
25. Jones, G. P. 1966. Spin-lattice relaxation in rotating frame: weak-collision case. *Phys. Rev.* 148:332–335.
26. Krushelnitsky, A., and D. Reichert. 2004. Response of lysozyme internal dynamics to hydration probed by C-13 and H-1 solid-state NMR relaxation. *Appl. Magn. Reson.* 27:501–518.
27. Goldman, M. 2001. Formal theory of spin-lattice relaxation. *J. Magn. Reson.* 149:160–187.
28. Lipari, G., and A. Szabo. 1982. Model-free approach to the interpretation of nuclear magnetic resonance relaxation in macromolecules. 1. Theory and range of validity. *J. Am. Chem. Soc.* 104:4546–4559.
29. Bertini, I., Y. K. Gupta, …, H. Schwalbe. 2005. NMR spectroscopic detection of protein protons and longitudinal relaxation rates between 0.01 and 50 MHz. *Angew. Chem. Int. Ed.* 44:2223–2225.
30. Krushelnitsky, A. G., and V. D. Fedotov. 1993. Overall and internal protein dynamics in solution studied by the nonselective proton relaxation. *J. Biomol. Struct. Dyn.* 11:121–141.
31. Krushelnitsky, A. 2006. Intermolecular electrostatic interactions and Brownian tumbling in protein solutions. *Phys. Chem. Chem. Phys.* 8:2117–2128.
32. Krushelnitsky, A. G., V. D. Fedotov, …, J. Straka. 1996. Dynamic structure of proteins in solid state. ^{1}H and ^{13}C NMR relaxation study. *J. Biomol. Struct. Dyn.* 14:211–224.
33. Blears, D. J., and S. S. Danyluk. 1968. Proton wide-line nuclear magnetic resonance spectra of hydrated proteins. *Biochim. Biophys. Acta.* 154:17–27.

34. Bova, M. P., L.-L. Ding, …, B. K.-K. Fung. 1997. Subunit exchange of αA-crystallin. *J. Biol. Chem.* 272:29511–29517.

35. Sedgwick, H., K. Kroy, …, W. C. Poon. 2005. Non-equilibrium behavior of sticky colloidal particles: beads, clusters and gels. *Eur Phys J E Soft Matter.* 16:77–80.

36. Strobl, G. 2007. The Pyhsics of Polymers, 3rd ed. Springer, Berlin-Heidelberg.

37. Nesmelova, I. V., V. D. Skirda, and V. D. Fedotov. 2002. Generalized concentration dependence of globular protein self-diffusion coefficients in aqueous solutions. *Biopolymers.* 63:132–140.

38. Horne, R. A., R. A. Courant, …, F. F. Margosian. 1965. The activation energy of viscous flow of pure water and sea water in the temperature region of maximum density. *J. Phys. Chem.* 69:3988–3991.

39. Ravera, E., G. Parigi, …, C. Luchinat. 2013. Experimental determination of microsecond reorientation correlation times in protein solutions. *J. Phys. Chem. B.* 117:3548–3553.

40. Zeeb, M., M. H. Jacob, …, J. Balbach. 2003. ^{15}N relaxation study of the cold shock protein CspB at various solvent viscosities. *Biomol. NMR.* 27:221–234.

41. Doliwa, B., and A. Heuer. 1998. Cage effect, local anisotropies, and dynamic heterogeneities at the glass transition: a computer study of hard spheres. *Phys. Rev. Lett.* 80:4915–4918.

42. Pusey, P. N. 2008. Colloidal glasses. *J. Phys. Condens. Matter.* 20:494202.

43. Mereghetti, P., and R. C. Wade. 2012. Atomic detail Brownian dynamics simulations of concentrated protein solutions with a mean field treatment of hydrodynamic interactions. *J. Phys. Chem. B.* 116:8523–8533.

44. Liang, J., and K. A. Dill. 2001. Are proteins well-packed? *Biophys. J.* 81:751–766.

45. Moret, M. A., M. C. Santana, …, G. F. Zebende. 2006. Protein chain packing and percolation threshold. *Physica A.* 361:250–254.

46. Banerji, A., and I. Ghosh. 2011. Fractal symmetry of protein interior: what have we learned? *Cell. Mol. Life Sci.* 68:2711–2737.

47. Fischer, H., I. Polikarpov, and A. F. Craievich. 2004. Average protein density is a molecular-weight-dependent function. *Protein Sci.* 13:2825–2828.

48. Harris, K. R., and L. A. Woolf. 2004. Temperature and volume dependence of the viscosity of water and heavy water at low temperatures. *J. Chem. Eng. Data.* 49:1064–1069.

49. Kestin, J., M. Sokolov, and W. A. Wakeham. 1978. Viscosity of liquid water in range −8°C to 150°C. *J. Phys. Chem. Ref. Data.* 7:941–948.

50. Tyn, M. T., and T. W. Gusek. 1990. Prediction of diffusion coefficients of proteins. *Biotechnol. Bioeng.* 35:327–338.

51. Ilyina, E., V. Roongta, …, K. H. Mayo. 1997. A pulsed-field gradient NMR study of bovine pancreatic trypsin inhibitor self-association. *Biochemistry.* 36:3383–3388.

52. Wilkins, D. K., S. B. Grimshaw, …, L. J. Smith. 1999. Hydrodynamic radii of native and denatured proteins measured by pulse field gradient NMR techniques. *Biochemistry.* 38:16424–16431.

53. Armstrong, J. K., R. B. Wenby, …, T. C. Fisher. 2004. The hydrodynamic radii of macromolecules and their effect on red blood cell aggregation. *Biophys. J.* 87:4259–4270.

Supporting Material

NMR-detected Brownian dynamics of αB-crystallin over a wide range of concentrations

Matthias Roos, Susanne Link, Jochen Balbach, Alexey Krushelnitsky,* Kay Saalwächter*

Institut für Physik, Martin-Luther-Universität Halle-Wittenberg,
Betty-Heimann-Str. 7, 06120 Halle (Saale), Germany.

Sample preparation.

Protein expression and purification of human αB-crystallin.

After cloning the human αB cDNA into a modified, His-tag free pET16b vector and expression in *Escherichia coli* BL21(DE3), protein expression and purification were performed in a manner similar to ref. (1). Briefly, αB-crystallin was expressed overnight at 22°C in the auto-induction media ZYM 5052, lysed by Microfluidizer in 20mM TrisHCL (pH 8.5) and 1mM EDTA buffer, the DNA digested by DNase1 and precipitated by protamine sulfate salt. After purification on a TMAE anion-exchange column with a stepwise NaCl gradient, αB fractions were pooled, concentrated and loaded on a S200 gel filtration column with a running buffer containing 20mM TrisHCL (pH 7.5), 50mM NaCl and 1mM EDTA. The purity of the protein was confirmed by SDS-page and mass spectrometry.

NMR sample preparation.

After extensive dialysis against 50mM ammonium hydrogen carbonate buffer (pH 8), the protein was lyophilized, then dissolved in the smaller amount of the same buffer in D_2O and lyophilized again. Note that multiple lyophilization does not affect αB-crystallin properties, as confirmed by NMR spectroscopic and diffusion experiments. The lyophilized αB-crystallin powder was

dissolved in 50mM Na-phosphate buffer, 50mM NaCl and 0.002% NaN_3 D_2O buffer at pH 7.6 (pD=7.2) and used in the NMR and viscosity measurements. The αB-crystallin concentration was determined by spectral photometry at 280 nm with MW=20027.7 Da and ε=13980 M cm^{-1}.

NMR experiments.

Translational diffusion

Translational self-diffusion coefficients were measured using the stimulated echo technique with bipolar pulsed field gradients (2). Fig. S1 shows proton spectra of αB-crystallin in D_2O buffer after a 90º-pulse (top). The strong signal at ~5 ppm corresponds to residual solvent protons that cannot be fully removed during the sample preparation. The NMR spectrum seen in the PFG experiments is shown at the bottom, in which the water signal is filtered out on the basis of its fast diffusion. A large fraction of the protein signal is also filtered out due to the short T_2 of the residues forming the rigid core, while the remaining signal belongs to the protons of mobile unstructured termini of αB-crystallin polypeptide chains that have long T_2. It is noted that without these unstructured termini the PFG measurement of translational diffusion would be impossible: αB-crystallin is a large protein, so its overall rotational tumbling is slow. If all parts of the protein were rigid, then the complete protein signal would be T_2-filtered (suppressed) during the field gradient pulse, which has a typical duration of 1 - 1.5 ms.

Analyses of the diffusion decay are based upon the right-hand side peak belonging to methyl protons, as marked by an arrow in Fig. S1. Fig. S2 compares the PFG NMR diffusion decay of the integral signal to that of the methyl protons peak. It is clearly seen that the two decays differ, with the difference becoming more pronounced at higher concentrations. Such a difference can be explained by the effect of spin diffusion between protein protons combined with hydrogen exchange of labile protein protons with the residual solvent protons. Thus, the apparent diffusion decay for the integral protein signal is distorted by the magnetic/chemical exchange processes (3,4). This effect is negligible in small and medium-sized proteins because spin diffusion is rather slow due to the much faster overall rotational tumbling, which averages out inter-proton dipole-dipole interactions. The methyl protons are less prone to such distortions since they undergo fast rotation around the C_3 axis, and thus have weak magnetic coupling to other protein protons.

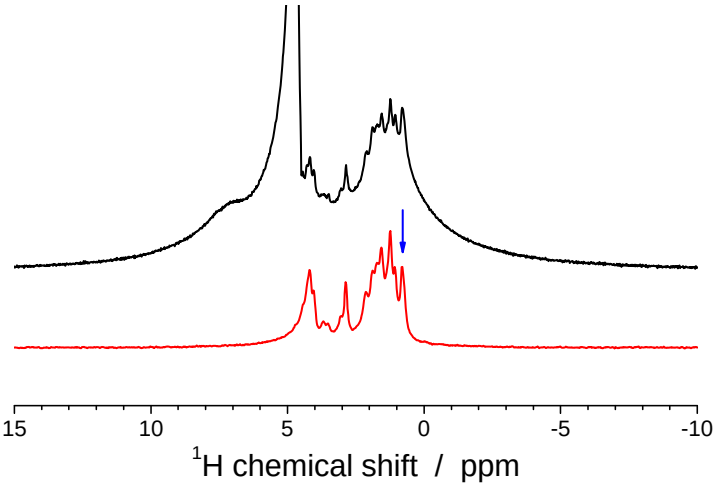

Figure S1. Proton NMR spectrum of αB-crystallin at 400 MHz resonance frequency after a 90º pulse (top), and after T_2/diffusion filtering during the pulse-gradient experiment (bottom). The blue arrow indicates the peak which was used for evaluating the diffusion decays.

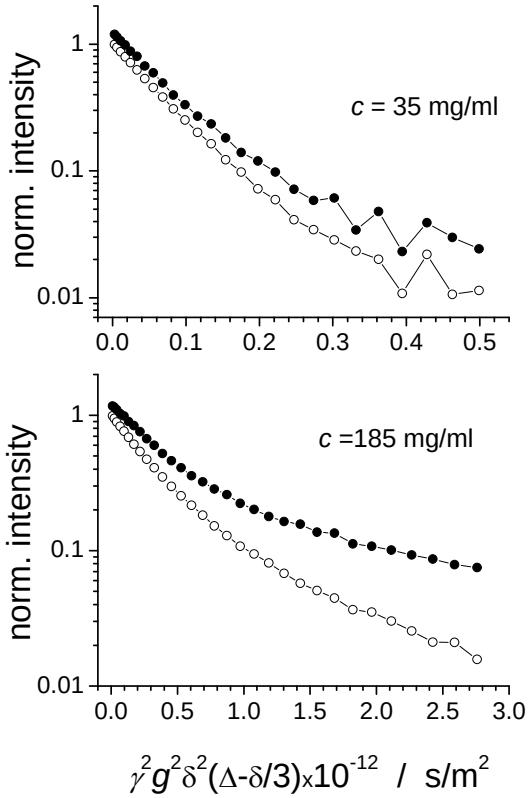

Figure S2. Diffusion decays for αB-crystallin solution at two concentrations (T = 20 ºC) plotted for the integral signal (open circles) and the methyl peak marked by an arrow in Fig. S1 (solid circles).

Fig. S3 compares the diffusion decays measured at two different diffusion times (Δ). The SDC should not depend on Δ, however, if the characteristic time of the magnetic/chemical exchange processes is comparable to Δ, then the apparent diffusion decay will become faster as Δ increases. It is seen that the diffusion decay at Δ = 300 ms is indeed somewhat faster, yet the difference is negligibly small. In our PFG experiments Δ was always between 25 and 40 ms, thus the effect of the magnetic/chemical exchange can be safely neglected.

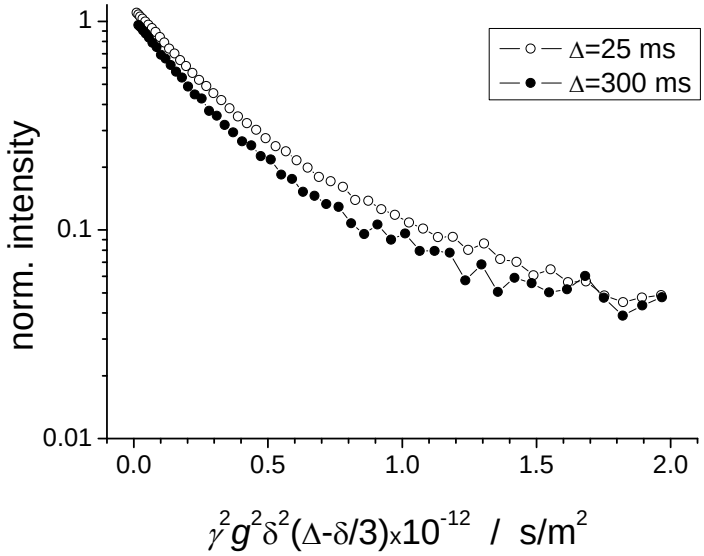

Figure S3. Diffusion decays measured at two different diffusion times (indicated in the plot) plotted for the methyl protons peak (c = 185 mg/ml, T = 28 ºC).

Spin relaxation

On-resonance $T_{1\rho}$'s at 20 and 40 kHz spin-lock frequencies were measured with the standard pulse sequence, Fig. S4. Off-resonance $T_{1\rho}$'s at 60 kHz were measured with the sequence shown in Fig. S5a. The latter sequence starts with two 90º-pulses, of which the first pulse is of fixed phase, while the second one is phase-alternated to ensure spin temperature inversion. In doing so, the relaxation signal decays exactly to zero, thus there is no need to measure the long relaxation delay plateau. In addition, the off-resonance spin-lock pulse is flanked by two orienting off-resonance 180º-pulses: the first orienting pulse aligns the magnetization vector along the B_{1e} field and the second one brings the magnetization back to B_0 direction. By this, the orienting pulse vector forms the angle $\theta/2$ with the B_0 (and B_{1e} as well) vector, see Fig. S5b.

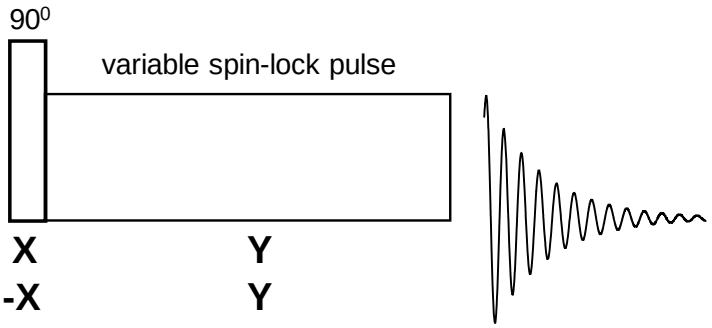

Figure S4. Pulse sequence for measuring $T_{1\rho}$ decays with on-resonance spin-lock field.

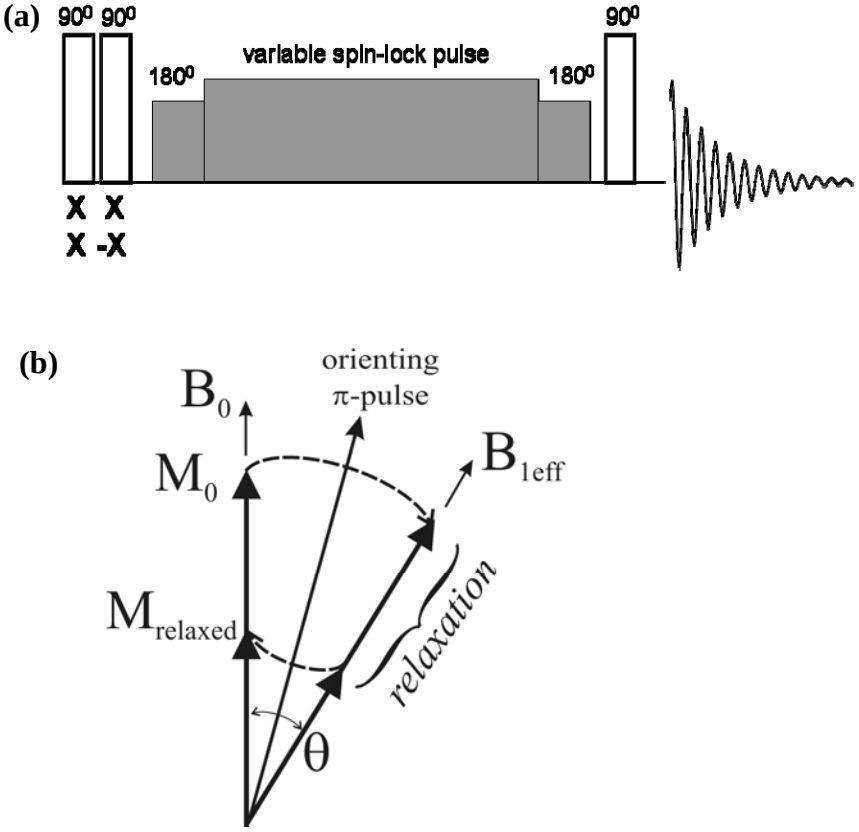

Figure S5. (a) Pulse sequence for measuring off-resonance $T_{1\rho}$. Shaded pulses are applied with the resonance offset. (b) Vector scheme demonstrating magnetization perturbations during the off-resonance pulses.

Before each $T_{1\rho}$ measurement the spin-lock frequencies and the angle θ (for the off-resonance experiments) were carefully calibrated using a nutation experiment. For all the off-resonance measurements the angle θ was equal to 42º. The spin-lock field duration in the $T_{1\rho}$ experiments

was varied from few μs to 200 ms. For plotting the relaxation decays, the whole spectral window (see Fig. S1, top) was used for integration of the proton signal. To avoid sample heating by long spin-lock pulses, the recycling delay was 20 s. The chemical shift of the residual water protons peak did not depend on the duration of the spin-lock pulse which confirms that the sample heating effect was negligible.

Spin-spin (T_2) relaxation decays were measured by a combination of three different experiments: Free induction decay (FID; time range from 12 (dead time) to 40 μs), Hahn echo (from 30 μs to ~3 ms) and a Carr-Purcell-Meiboom-Gill sequence (from 0.5 ms to ~0.4 s). This was done in order to cover a wide range of the relaxation times, as the protein T_2 is very short, usually tens to hundreds of μs, whereas the solvent T_2 was of the order of hundreds of ms. Since T_2 relaxation decays were measured at the resonance frequency 20 MHz and imperfect B_0 field homogeneity, no spectral resolution could be achieved at these conditions and thus, the decays were recorded directly in the time domain.

The analysis of the $T_{1\rho}$ and T_2 relaxation decays was performed according to the procedure described in ref. (5). As mentioned above, protein solutions contain a certain amount of residual solvent protons which exhibit much longer $T_2/T_{1\rho}$'s, thus requiring to subtract the solvent signal for analyzing the unbiased protein signal (cf. Fig. S6). For plots and analyses, the relaxation decays of the total (integral) proton signal was detected without any spectroscopic separation in both the $T_{1\rho}$ and T_2 experiments. The water signal subtraction procedures (Fig. S6) for the T_2 and $T_{1\rho}$ decays were fully identical.

After subtraction of the solvent signal we obtained the protein protons' relaxation decay, which is of multi-exponential shape (Fig. S6). This decay reflects a wide distribution of the relaxation times which is a consequence of the dynamic heterogeneity of α-crystallin. For such a decay we determined the mean relaxation rate/time, which equals the slope of the initial part of the decay. In practice, we fitted the decays with a sum of two exponential components, which provides a minimal fitting model. We then determined the mean relaxation rate as

$$\left\langle \frac{1}{T_2} \right\rangle = \frac{1}{P_a + P_b}\left(\frac{P_a}{T_{2a}} + \frac{P_b}{T_{2b}} \right),$$

where $P_{a,b}$ and $T_{2a,b}$ are the intensities and relaxation times of the two components, respectively (taken separately, these parameters have no physical meaning).

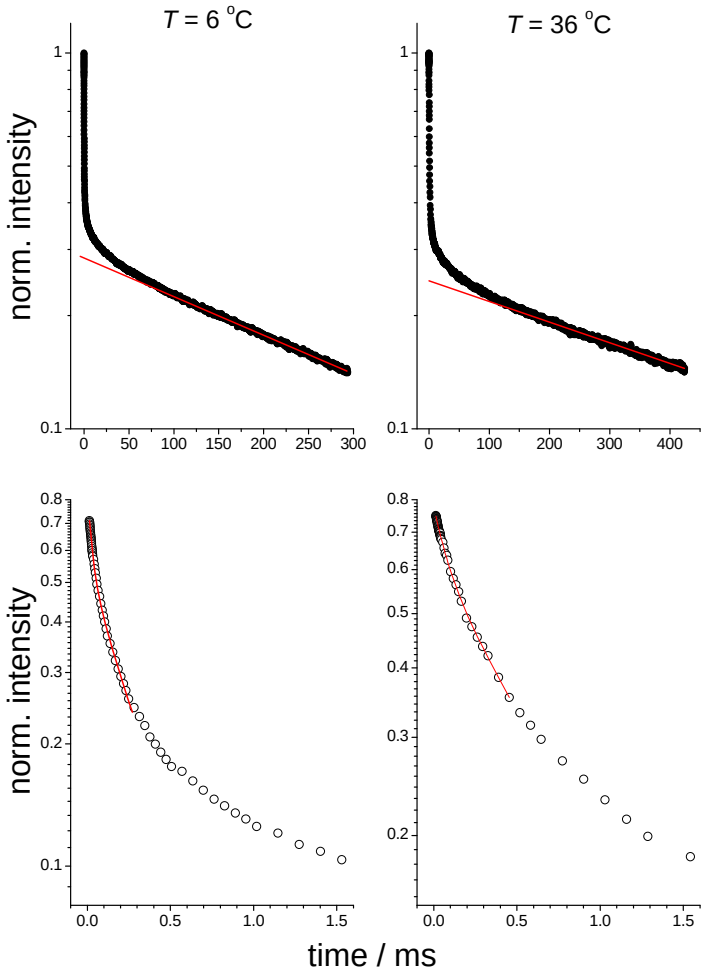

Figure S6. T_2-relaxation decays measured for αB-crystallin solutions at c =80 mg/ml and two temperatures (indicated in the figure). $T_{1\rho}$-decays have very similar shapes. *Top:* raw relaxation decays consisting of the fast (protein) and slow (solvent) relaxing components. Red lines indicate the solvent component that was defined from the exponential fit of the slow tail of the relaxation decay. *Bottom:* the protein relaxation signal after the subtraction the solvent component from the overall decay. Red curves correspond to the biexponential fit of the initial part of the decay, which was used for the determination of the mean relaxation time (initial slope of the decay) as described in the text. Possible cross-relaxation (spin diffusion) between protein protons may change the form of the relaxation decay, but the mean relaxation rate (initial slope) does not depend on this.

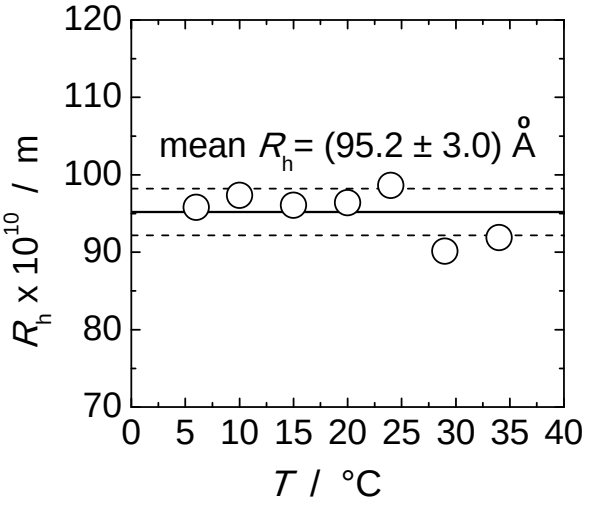

Figure S7. Hydrodynamic radii of αB-crystallin as determined via the Stokes-Einstein relationship with independent measurements of the viscosity and translational self-diffusion at a concentration of 35 mg/ml. The solid and dashed lines indicate the mean value of all points and their standard deviation, respectively.

Fitting the temperature dependences of the relaxation times: (i) distribution of correlation times. Taking into account the intrinsic size distribution of α-crystallin, as also reflected in the PFG NMR diffusion decays, it is worthy to estimate the impact of a distribution of τ_{rot} on the fitting result of the T_2 and $T_{1\rho}$ data. To simulate a τ_{rot} distribution, the fast component was represented by a spread of 3 modes on a logarithmic scale, namely 2/3 $\tau_{rot,}$ τ_{rot}, and 3/2 $\tau_{rot,}$ with relative amplitudes of ¼, ½ and ¼ for the faster, main and slower component, respectively. The total spectral density function addressing the fast component thus reads

$$J_{fast}(\omega;\tau_{rot}) = \tfrac{1}{4} J(\omega;\tfrac{2}{3}\tau_{rot}) + \tfrac{1}{2} J(\omega;\tau_{rot}) + \tfrac{1}{4} J(\omega;\tfrac{3}{2}\tau_{rot})$$

and reflects a relative standard deviation of τ_{rot} of approx. 35%. As a consequence, this broadens the minimum of the $T_{1\rho}$ curves, yet such a spread of τ_{rot} values was not found to have an appreciable effect on the quality of the fitting result (cf. Fig. S8) and the fitting values obtained (cf. Table S1). In fact, the relative increase of the mean τ_{rot} was found to be in good accordance with the previous results when modeling the experimental data using a single value of τ_{rot} only. Thus, introducing a spread of τ_{rot} is not reasonable since it does not change significantly the fitting

results, at the same time making fitting less certain by increasing the number of fitting parameters.

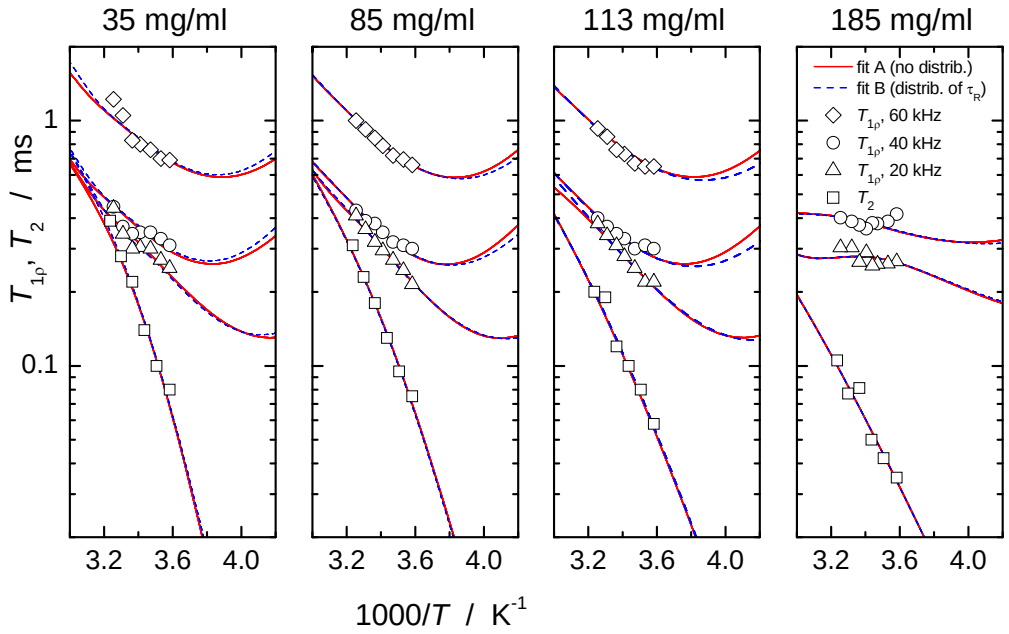

Figure S8. T_2 and $T_{1\rho}$ relaxation times (see legend) with their best fit results (lines) by use of a distribution of the fast component τ_{rot} (dashed lines) in comparison to the fitting result using a single value of τ_{rot} (solid lines).

Table S1. Summary of the fitting result by reflecting the fast component (τ_{rot}) by one mode only (model A) in comparison to the outcome assuming a logarithmic spread of τ_{rot} with a standard deviation of about 35% (model B, see explanation in the text). $<\tau_{rot}>$ for the model (B) was calculated as $\langle\tau_{rot}\rangle^{-1} = \frac{1}{4}\left(\frac{2}{3}\tau_{rot}\right)^{-1} + \frac{1}{2}(\tau_{rot})^{-1} + \frac{1}{4}\left(\frac{3}{2}\tau_{rot}\right)^{-1}$. $\langle R_{rot}\rangle$ was calculated according to Eq. 11 of the main paper.

Model	τ	35 mg/ml	85mg/ml	113 mg/ml	185mg/ml
(A)	τ_{rot} / μs	0.90±0.02	0.96±0.02	1.03±0.02	1.04±0.02
	$\langle R_{rot}\rangle^{-1}$ / μs	0.91±0.05	0.98±0.05	1.05±0.05	1.31±0.05
	$\langle R_{rot}\rangle(c_1)/\langle R_{rot}\rangle(c_i)$	**1.00**	**1.08±0.02**	**1.15±0.02**	**1.44±0.04**
(B)	$<\tau_{rot}>$ / μs	0.85±0.02	0.89±0.02	0.97±0.02	0.96±0.02
	$\langle R_{rot}\rangle^{-1}$ / μs	0.86±0.05	0.91±0.05	0.99±0.05	1.17±0.05
	$\langle R_{rot}\rangle(c_1)/\langle R_{rot}\rangle(c_i)$	**1.00**	**1.05±0.02**	**1.16±0.02**	**1.36±0.04**

Fitting the temperature dependences of the relaxation times: (ii) K_{HH}^{av} temperature dependence. In the analysis we assume K_{HH}^{av} to be temperature independent although the amplitude of internal motions in proteins may depend on temperature (6,7). To check the influence of the possible K_{HH}^{av} temperature dependence on the fitting results, we performed the fitting assuming a simple linear dependence of K_{HH}^{av} on temperature. Direct measurements of K_{HH}^{av} in solid hydrated proteins at different temperatures (8,9) show that within temperature range of our experiments (from ~5 ºC to ~35 ºC) K_{HH}^{av} varies no more than 10-20%. Note that this temperature variation is caused not only by the change of motional amplitude, but mainly by the temperature dependence of the correlation times of internal motions which affects the motional averaging of the proton second moment. Therefore, we fitted the data assuming the 15% difference of K_{HH}^{av} between 5 and 35 ºC. The fitting curves in this case look the same as in Fig. S8 or Fig. 3 of the main paper. The comparison of the fitting results (Table S2) with those assuming temperature independent K_{HH}^{av} (Table 1 of the main paper) demonstrates that the K_{HH}^{av} temperature dependence affects only the absolute value of K_{HH}^{av} and the activation energy E_{rot}. All other parameters remain the same.

Table S2. Dynamic parameter obtained from the fitting assuming K_{HH}^{av} to be temperature dependent. K_{HH}^{av} at 20 ºC is $(3.7\pm0.1)\cdot10^{9}$ s^{-2}.

c / mg/ml	τ_{rot} / μs at 20 ºC	$S_{\mathrm{rot}}^2\ \tau_{\mathrm{S}}$ / μs at 20 ºC	E_{rot} / kJ/mol	E_{s} / kJ/mol
35	0.92±0.02	0.65±0.02	12±1	63±2
85	0.97±0.02	0.84±0.02	13±1	49±2
113	1.04±0.03	1.38±0.03	12±1	38±2
185	1.07±0.03	3.73±0.07	2±1	27±1

Here, we would like to also demonstrate that the assumption of the possibly steeper temperature dependence of K_{HH}^{av} cannot describe the data well without taking into account the slow component of the $C_t(t)$, i.e. assuming S_{rot}^2 =0. We performed the data fitting assuming S_{rot}^2 =0 and the slope of the K_{HH}^{av} temperature dependence as an additional free fitting parameter. As a result, we obtained a bad fitting quality (see Fig. S9) and a rather unreasonable temperature variation of K_{HH}^{av} of about 40% between 5 and 35 ºC. Thus, the assumption of the K_{HH}^{av} temperature dependence has no significant influence on our results.

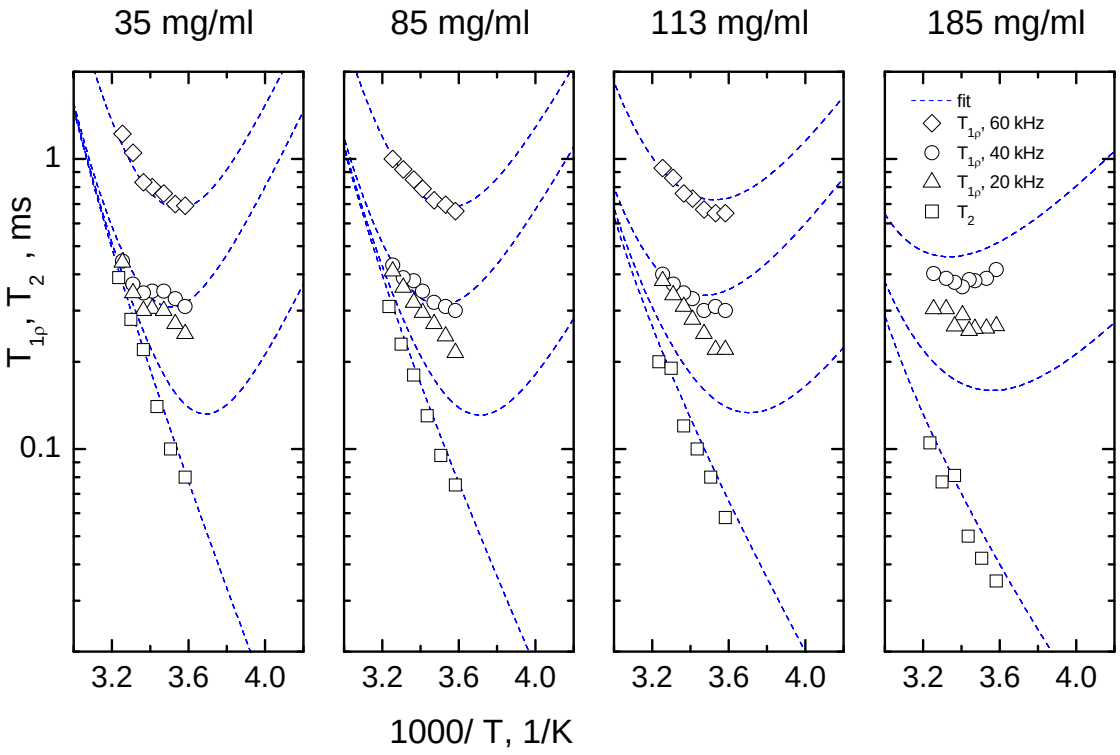

Figure S9. Fitting results assuming K_{HH}^{av} to be temperature-dependent, and S_{rot}^2 =0.

Fitting the temperature dependences of the relaxation times: (iii) fixed ratio between the correlation times. Fig. S10 shows fits for which we tried a ratio between the correlation times fixed to

τ_{rot}(35 mg/ml): τ_{rot}(85 mg/ml): τ_{rot}(113 mg/ml): τ_{rot}(185 mg/ml) = 1.00 : 1.67 : 2.20 : 6.00,

which corresponds to the relative increase in viscosity (or the translational diffusion slow-down). Obviously, this results in a strong mismatch between the fitting curves and the experimental data.

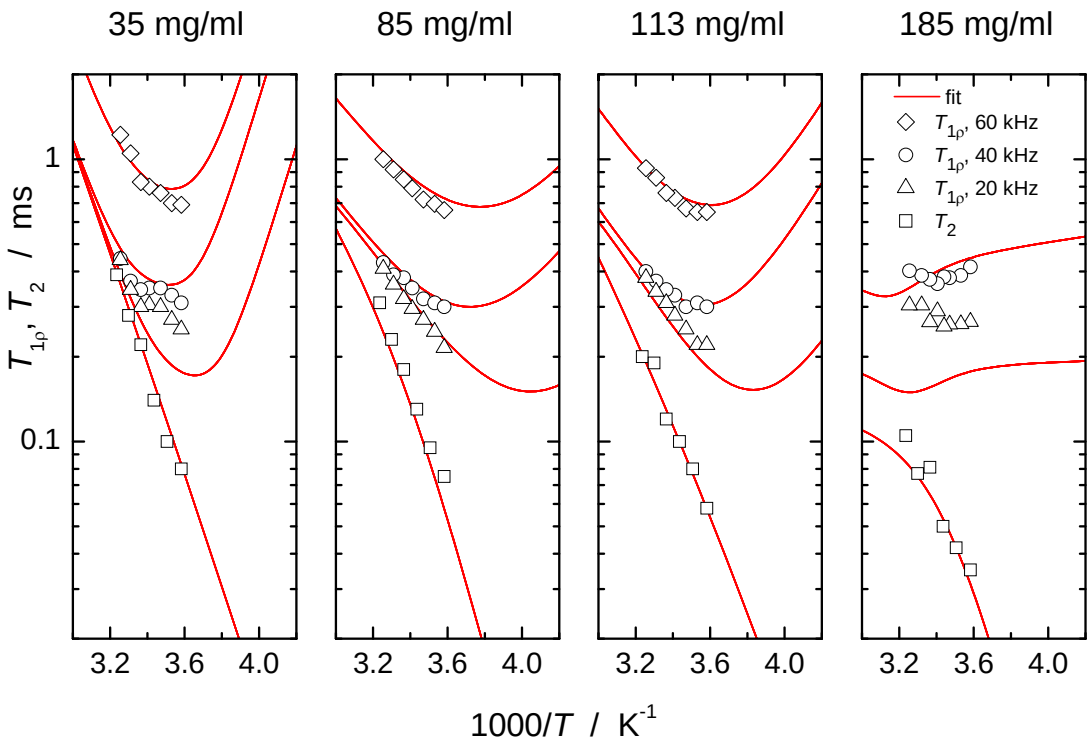

Figure S10. T_2 and $T_{1\rho}$ relaxation times with their best fit results (red lines) by use of a fixed ratio of the rotational correlation time τ_{rot} following the retardation of translational diffusion.

Rotational correlation time vs. molecular mass: statistics of literature data.

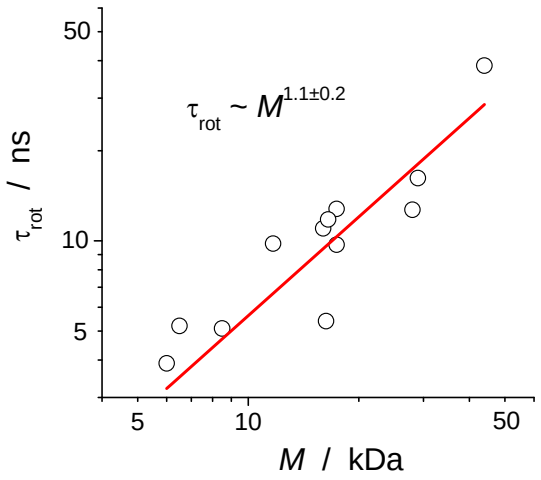

Figure S11. Rotational correlation time as a function of the protein M for 12 different proteins. All correlation times were recalculated for the temperature 20 ºC, the details being presented in Table S3. It is clearly seen that the slope can be defined only with a large uncertainty.

Table S3. Collection of rotational correlation times for 12 different proteins. In all cases the correlation time was defined from the ^{15}N T_1/T_2 ratio. Since the temperatures of the measurements were different, all the correlation times were recalculated to 20 ºC using the Arrhenius dependence and an activation energy of 20 kJ/mol. Fig. S8 was plotted using the numbers in bold (2nd and 5th columns).

Protein	MM, kDa	T / ºC	τ_{rot} / ns	τ_{rot} (20ºC)	Reference
Interleukin 1β	**17.4**	36	8.3	**12.8**	Clore GM, Driscoll PC, Wingfield PT, Gronenborn AM (1990), *Biochemistry* 29: 7387–7401.
calbindin D9k	**8.5**	27	4.2	**5.1**	Kordel J, Skelton NJ, Akke M, Palmer AG, Chazin WJ (1992), *Biochemistry* 31: 4856–4866.
Bacillus-subtilis glucose perme-ase-IIA domain	**17.4**	35	6.5	**9.7**	Stone MJ et al. (1992), *Biochemistry* 31: 4394–4406.
Thioredoxin	**11.7**	35	6.55	**9.8**	Stone MJ, Chandrasekhar K, Holmgren A, Wright PE, Dyson HJ (1993), *Biochemistry* 32: 426–435.
Interleukin-8	**16**	27	9.1	**11.0**	Grasberger BL, Gronenborn AM, Clore GM (1993), *J Mol Biol* 230: 364–372.
Igg binding domain	**6**	26	3.3	**3.9**	Barchi JJ, Jr., Grasberger B, Gronenborn AM, Clore GM (1994), *Prot Sci* 3: 15–21.
Ribonuclease HI	**16.5**	27	9.7	**11.8**	Mandel AM, Akke M, Palmer AG (1995), *J. Mol Biol* 246: 144–163.
Savinase	**28**	30	9.7	**12.7**	Remerowski ML, Pepermans HAM, Hilbers CW, Van De Ven FJM (1996), *Eur J Biochem* 235: 629–640.

SH3 domain	**6.5**	7	7.6	**5.2**	Chevelkov V, Zhuravleva AV, Xue Y, Reif B, Skrynnikov NR (2007), *J Am Chem Soc* 129: 12594–12595.
Flavodoxin	**16.3**	27	4.5	**5.4**	Hrovat A, Blümel M, Löhr F, Mayhew SG, Rüterjans H (1997), *J Biomol NMR* 10: 53–62.
Ectodomain of SIV gp41	**44**	45	20	**38.5**	Caffrey M, Kaufman J, Stahl SJ, Wingfield PT, Gronenborn AM, Clore GM (1998), *J Magn Reson* 135: 368 –372.
TEM-1 β-lactamase	**29**	30	12.4	**16.2**	Savard PY, Gagne SM (2006), *Biochemistry 45*: 11414-11424.

References.

(1) Mainz, A., S. Jehle, B.J. van Rossum, H. Oschkinat, and B. Reif (2009). Large protein complexes with extreme rotational correlation times investigated in solution by magic-angle-spinning NMR spectroscopy. *J Am Chem Soc* 131: 15968-15969. (Supporting Information)

(2) Cotts R.M., M.J.R. Hoch, T. Sun, and J.R. Markert (1989). Pulsed Field Gradient Stimulated Echo Methods for Improved NMR Diffusion Measurements in Heterogeneous Systems. *J Magn Reson* 83: 252-266.

(3) Chen A., C.S. Johnson Jr., M. Lin, and M.J. Shapiro (1998). Chemical Exchange in Diffusion NMR Experiments. *J Am Chem Soc* 120: 9094-9095.

(4) Andrec M, and J.H. Prestegard (1997). Quantitation of chemical exchange rates using pulsed-field-gradient diffusion measurements. *J Biomol NMR* 9: 136-150.

(5) Krushelnitsky, A.G., and V.D. Fedotov (1993). Overall and internal protein dynamics in solution studied by the nonselective proton relaxation. *J Biomol Struct Dyn* 11:121-141.

(6) Chang, S.-L., and N. Tjandra (2005). Temperature dependence of protein backbone motion from carbonyl ^{13}C and amide ^{15}N NMR relaxation. *J Magn Reson* 174: 43-53.

(7) Johnson, E, A.G. Palmer, and M. Rance (2007). Temperature dependence of the NMR generalized order parameter. *Prot Str Func Bioinf* 66: 796-803.

(8) Blears, D.J and S.S.Danyluk (1968). Proton wide-line nuclear magnetic resonance spectra of hydrated proteins. *Biochim Biophys Acta* 154: 17-27.

(9) Krushelnitsky, A.G., V.D. Fedotov, J. Spevacek, and J. Straka (1996). Dynamic structure of proteins in solid state. ^{1}H and ^{13}C NMR relaxation study. *J Biomol Struct Dyn* 14: 211-224.